

# The quantum defect: the true measure of time-dependent density-functional results for atoms

Meta van Faassen and Kieron Burke

*Department of Chemistry and Chemical Biology, Rutgers University  
610 Taylor Rd., Piscataway, NJ 08854-8087, USA*

(Dated: November 20, 2018)

Quantum defect theory is applied to (time-dependent) density-functional calculations of Rydberg series for closed shell atoms: He, Be, and Ne. The performance and behavior of such calculations is much better quantified and understood in terms of the quantum defect, rather than transition energies.

## I. INTRODUCTION

Time-dependent density functional theory (TDDFT) [1] has enjoyed a recent surge in popularity for calculating excited-state energies of atoms, molecules, clusters, and solids [2, 3]. TDDFT has features similar to ground-state density functional theory (DFT): It produces useful accuracy at a fraction of the computational cost of *ab initio* methods [2], but reliability depends on the approximate functionals used [4]. As more and more practitioners in many subfields of computational science use TDDFT, there are ever increasing numbers of implementations. Calculations on atoms and sequences of atoms are often used to benchmark new implementations, or to show how well TDDFT works in the simplest cases. These are particularly useful, as much highly accurate data, both from experiment and accurate wave function calculations, are available for these systems.

A well-known difficulty that hampered even the earliest calculations of excitations in atoms with TDDFT [5] is the incorrect asymptotic behavior of the ground-state potentials of common density functional approximations. It has long been known that the exact KS potential for a closed shell atom decays as  $-1/r$  at large  $r$ , where  $r$  is the distance from the nucleus [6, 7]. Typical approximations for the ground-state, such as the local density approximation (LDA), gradient corrected functionals (GGAs), and hybrid functionals (see for example Ref. [8] and references therein), have potentials that decay too rapidly with  $r$ . Only those with the correct asymptotic behavior support the Rydberg series of transitions, an infinite number of transitions that merge with the continuum at the ionization threshold. Orbital-dependent functionals capture this behavior naturally, as does the Van Leeuwen-Baerends potential approximation (LB94) [9], which was designed to have an asymptotically correct behavior. Several recent methods have been suggested for correcting the standard functionals to produce the long-ranged tail [10, 11, 12]. In any event, our present work applies only to long-ranged potentials.

We argue here that the way in which results have been calculated and reported for atoms is far from optimal. We show that long lists of transition frequencies for Rydberg series converging to the ionization threshold are *not* the

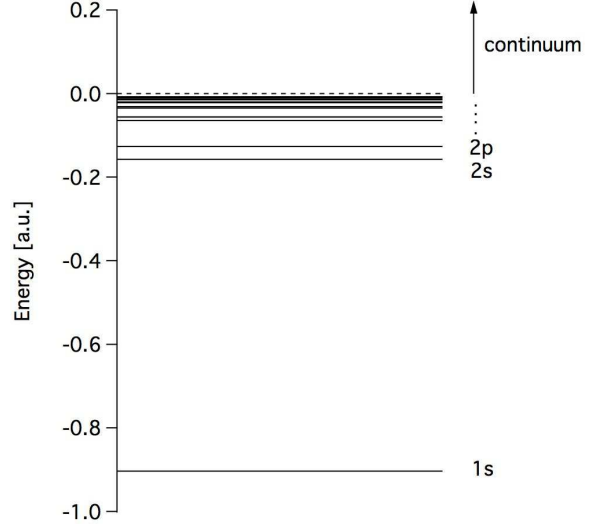


FIG. 1: Energy level diagram for the helium atom.

best way to report such calculations. Instead, the well-developed theory of the quantum defect [13], used for decades in atomic physics, is ideal for this purpose. We show that, for each Rydberg series, i.e., for each value of angular momentum  $l$ , two or three numbers completely characterize all the information in the infinite series. Furthermore, the quantum defect is a much more demanding test of excitation energies, and methods that appear to have only small energetic errors can yield quite poor quantum defect behavior. Also, shifts in orbital energies, such as the missing correlation contribution in the exact exchange HOMO energy, have no effect on the quantum defect, so that the quality of a potential can be assessed without being influenced by such errors. We also find [14], that the quantum defect of the exact ground-state Kohn-Sham (KS) potential, is sometimes, but not always, a good starting point for approximations to the true quantum defect.

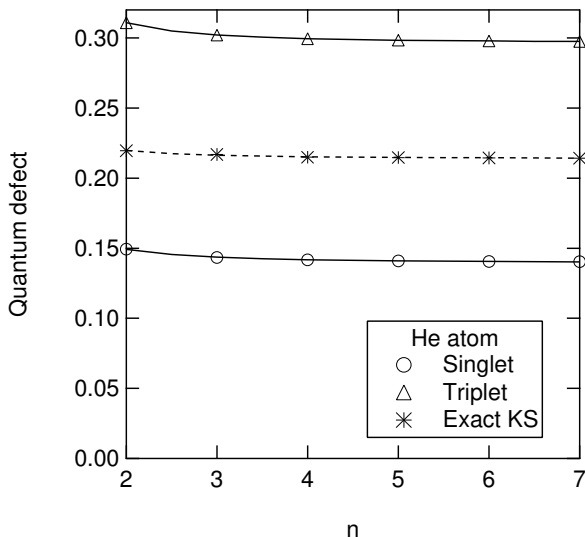


FIG. 2: The exact  $s$  KS quantum defect and the exact singlet and triplet quantum defects [16] of He and their parabolic fits.

## II. THEORY

In Fig. 1 we show the orbital energy level diagram of the helium atom. The zero is set at the onset of the continuum, marked with a dotted line. For closed shell atoms and for any spherical one-electron potential that decays as  $-1/r$  at large distances, the bound-state transitions form a Rydberg series with frequencies:

$$\omega_{nl} = I - \frac{1}{2(n - \mu_{nl})^2} \quad (1)$$

where  $I$  is the ionization potential, and  $\mu_{nl}$  is called the quantum defect. We use atomic units ( $e^2 = \hbar = m_e = 1$ ) throughout. The value of the quantum defect is that, for real atoms, quantum defects depend only weakly on the principle quantum number  $n$  for large  $n$  and converge to a finite value in the limit  $n \rightarrow \infty$ . In fact, according to Seaton's theorem [15], the quantum defect is a smooth function of energy as  $E \rightarrow 0$ , and merges continuously with the phase-shift (relative to pure Coulomb scattering) divided by  $\pi$ . In Table I, we report extremely accurate results from wavefunction calculations for the helium atom. We show singlet and triplet values that have been obtained by Drake [16]. We also give results from the exact ground-state KS potential, as found by Umrigar and Gonze [17]. We say more on how we obtained the KS values in section III A. On the left are the transition frequencies, while on the right are the corresponding quantum defects. Note how small the differences between transitions become as one climbs up the ladder, and yet the quantum defect remains finite and converges to a definite value.

In Fig. 2 we show the exact  $s$  KS quantum defect and the singlet and triplet quantum defects corresponding to accurate wave function results [16] for helium as sym-

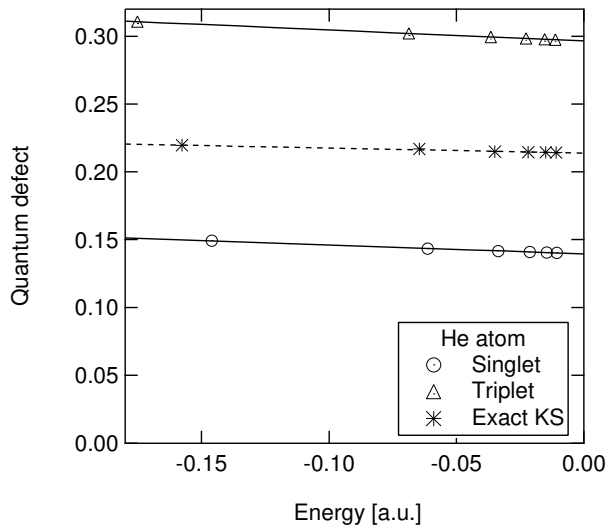


FIG. 3: Same as Figure 2 plotted against energy.

bols. This is the way the defect was plotted in Ref. [14] for the case of the Ne atom. However, it is more appropriate still to plot the defect as a function of energy, as shown in Fig. 3. This clearly illustrates that the quantum defect is a smooth function of energy, and will be well approximated a polynomial of some low order  $p$ :

$$\mu^{(p)}(E) = \sum_{i=0}^p \mu_i E^i, \quad E = \omega - I. \quad (2)$$

We choose to optimize the fit over the entire range of excitation energies, not just about  $E = 0$  (the  $\mu_i$  are simply related to the  $a$ ,  $b$ , and  $c$  coefficients in Ref. [14]). For example the data in Fig. 3 can be accurately described by a straight line. We report these coefficients in Table II and give the quantum defects obtained from these coefficients as continuous lines in Figs. 2 and 3. We also added the transition energies for He obtained from the KS fit to Table I. The maximum error in the fit is 3/100 mH so it is essentially exact for all purposes of this paper. We shall see that in other cases just two or even three coefficients are not enough to describe the data accurately. In those cases we will need to decide when to stop adding more coefficients to fit the data, since we would like to describe the data with as few coefficients as possible. Therefore we will look at the maximum absolute error in the quantum defect. By which we mean that we recalculate the quantum defects from the coefficients and look at the absolute differences between the fitted and original values, and then look at the largest difference. We will stop adding more coefficients once the maximum absolute error is smaller than 0.001, or, in case this value is not reached, whenever the absolute errors do not change much when adding more coefficients. We give the value for the error also in Table II. Any approximate ground-state KS potential suggested for use in TDDFT should have its coefficients compared with the KS num-

TABLE I: Transition energies for He atom [a.u.]. The ionization energies are 0.9037244 a.u. for the singlet and triplet case and 0.90372 a.u. for the KS potential.

Transition	$\Delta E$				Quantum defect		
	Singlet <sup>a</sup>	Triplet <sup>a</sup>	KS <sup>b</sup>	KS fit	Singlet	Triplet	KS
1s → 2s	0.7577503	0.7284949	0.74599	0.74596	0.1492525	0.3107982	0.21957
1s → 3s	0.8424524	0.8350353	0.83917	0.83920	0.1433699	0.3020047	0.21689
1s → 4s	0.8701376	0.8672122	0.86883	0.86882	0.1416535	0.2994464	0.21492
1s → 5s	0.8825475	0.8883469	0.88189	0.88189	0.1409171	0.2983583	0.21459
1s → 6s	0.8891613	0.8925944	0.88879	0.88879	0.1405330	0.2977954	0.21441
1s → 7s	0.8930986	0.8925945	0.89287	0.89287	0.1403072	0.2974666	0.21429

<sup>a</sup>Accurate non-relativistic calculations from Ref. [16].

<sup>b</sup>The differences between the KS eigenvalues obtained with the exact potential from Ref. [17].

TABLE II: Fit coefficients  $\mu_0$ , and  $\mu_1$  for the  $s$  quantum defect of He. By ‘Max. AE’ we mean the maximum absolute error as explained in the text.

	Singlet <sup>a</sup>	KS <sup>b</sup>	Triplet <sup>a</sup>
$\mu_0$	0.1396	0.2139	0.2965
$\mu_1$	-0.0655	-0.0370	-0.0811
Max. AE	0.0002	0.0006	0.0001

<sup>a</sup>Obtained from non-relativistic calculations of the orbital energies from Ref. [16].

<sup>b</sup>KS values obtained with the exact potential from Ref. [17].

bers in the table, while any approximate xc-kernel should have its coefficients compared with the singlet and triplet case.

### III. GROUND-STATE KOHN-SHAM POTENTIALS

All linear response TDDFT calculations of excitations begin from the occupied to unoccupied transitions of the *ground-state* KS potential. In this section, we analyse some of the most popular approximations using quantum defect theory.

#### A. Computational details

All ground-state DFT results shown here are calculated with a modified OEP (optimized potential model) program [18, 19, 20]. This program is basis set independent, works with a radial grid, and both the energies and the potentials are optimized in a self-consistent way. The exact-exchange (x-only) OEP is already included in this program. We also did calculations with the LB94 [9] potential by Van Leeuwen and Baerends, which was not available in the program. We implemented this functional by adding the LB94 correction to the LDA xc-potential and let the program optimize this potential in a self consistent manner. The program has the ability to read in the accurate potentials by Umrigar *et al.* (He [17], Be [21], and Ne [21]). These accurate potentials

TABLE III: The  $\mu_i$  from the exact ground-state KS potential for He, Be, and Ne.

	He <sup>a</sup>	Be <sup>b</sup>	Ne <sup>b</sup>
$s$			
I	0.9037	0.3426	0.7945
$\mu_0$	0.2139	0.7164	1.3125
$\mu_1$	-0.0370	-0.2185	-0.1807
Max. AE	0.0006	0.0002	0.0007
$p$			
$\mu_0$	0.0164	0.3587	0.8304
$\mu_1$	0.0289	-0.3377	-0.3500
$\mu_2$		0.6112	
Max. AE	0.0009	0.0003	0.001

<sup>a</sup>Ref. [17]

<sup>b</sup>Ref. [21]

were only known by us up to a particular radius. In order to calculate energies for higher  $n$  values we needed to increase this radius. We did this by adding a  $-1/r$  tail to  $v_{xc}$  and a  $Z/r$  tail to  $v_{rmH}$  and we checked that the transition was smooth. We also made sure our values are converged with the number of gridpoints. When we used the accurate potentials, we did not allow the program to self consistently change the potential.

The maximum  $n$  value for which we could still do very accurate calculations is  $n = 7$  for He and  $n = 9$  for Be and Ne.

#### B. Exact results

As we have seen the numbers,  $\mu_i$ , contain all the information needed to characterize a given Rydberg series, and make tables of the actual transition frequencies redundant. In Table III, we report the coefficients for  $s$  and  $p$  KS quantum defects for the He, Be and Ne atoms obtained with accurate xc potentials. We use the transitions up to  $n = 9$  for the fit in case of Be and Ne, and up to  $n = 7$  in case of He.

When we compare the  $s$  ( $l = 0$ ) values with  $p$  ( $l = 1$ ), the asymptotic KS quantum defect is smaller for  $p$  in all cases. This reflects the lesser importance of the inner part of the KS potential relative to the angular momentum

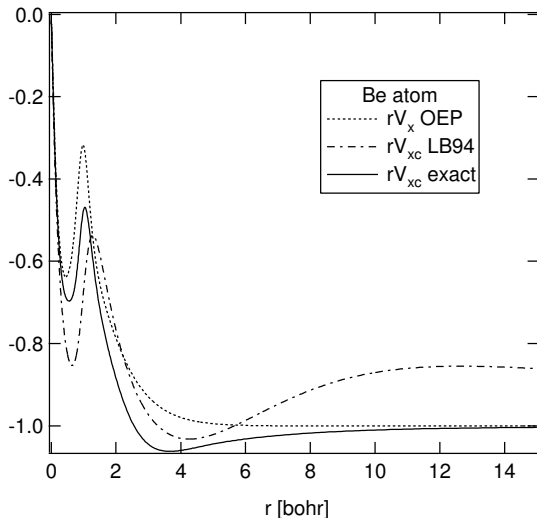


FIG. 4: The exact, LB94, and x-only potentials for beryllium together with  $-1/r$ .

barrier as  $l$  grows. However, the curvature of the  $s$  and  $p$  quantum defect is similar.

### C. Approximations

In this section, we demonstrate our methodology by testing two common approximations for the ground-state KS potential. These are exact exchange OEP [20] and LB94 [9]. Exact exchange calculations are more demanding than traditional DFT calculations, but are becoming popular because of the high quality of the potential [22, 23]. On the other hand, LB94 provides an asymptotically correct potential at little extra cost beyond traditional DFT [11, 24, 25]. Fig. 4 shows both these potentials for the Be atom together with the exact potential [21]. Our figure for the exact potential is different from the one in Ref. [9], since in that reference they use a different accurate density to derive the potential. We give our values for the fit parameters in Table IV. In Fig. 5 we show the  $p$  Be quantum defect obtained with LB94, OEP, and KS and we show the fit as continuous lines. Fig. 5 immediately shows the high quality of the OEP potential. The quantum defect curve is almost identical to the exact one, being offset by about 0.1 (see Table IV). On the other hand the quantum defect of LB94 is poor, and this is true for all cases studied. From Fig. 4 we can see that the OEP is much closer to the true potential than LB94 and also approaches  $-1/r$  faster. This shows that just having a potential that is asymptotically correct is not enough to get a good quantum defect.

Another thing we have not mentioned so far is that a potential that gives a wrong ionization potential does not necessarily give a bad quantum defect. The origin of this is that the quantum defect is obtained from  $\omega_{nl} - I$  and can take a shift of energy levels into account. Con-

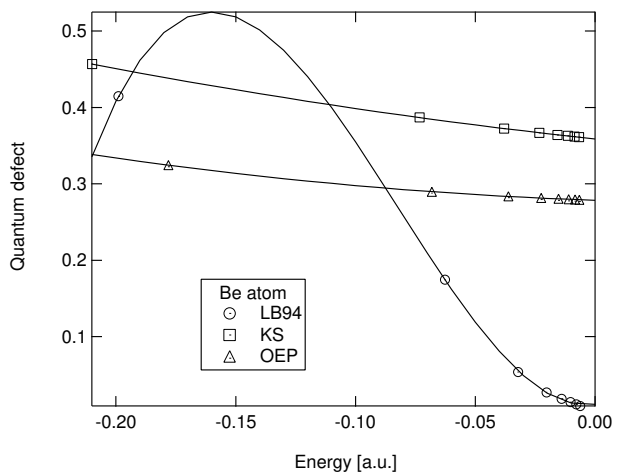


FIG. 5: The Be  $p$  quantum defect of LB94, OEP, and KS, and their best fits.

sider the exact exchange results for the atoms. Typically, these quantum defects are accurate to 0.1. Thus, using the exact ionization potential with the exchange quantum defects, yields highly accurate transition frequencies, i.e., the most significant error in OEP excitations is due to the missing correlation contribution to the position of the HOMO. On the other hand, we see that LB94, while asymptotically correct and sometimes having a highly accurate ionization potential, has much less accurate quantum defects.

## IV. TDDFT RESULTS

In the previous sections we saw that the KS quantum defects are typically lying in between the exact singlet and triplet quantum defects [31]. In order to calculate these singlet and triplet quantum defects within DFT the usual method of choice is TDDFT (within the linear response regime). Apart from a ground-state potential one needs to choose an xc-kernel as well. In this section we obtain quantum defects from excitation energies obtained with different xc-kernels and ground-state potentials. We focus mainly on the Be atom, but we also give expansion coefficients for He and Ne quantum defects.

### A. Performance of TDDFT

We concentrate on the quantum defect obtained from the ALDA kernel applied to the exact ground-state KS potential. In Table V, we show  $s \rightarrow s$  and  $s \rightarrow p$  excitation energies for the Be atom. The ALDA results in column three are obtained by Van Gisbergen *et al.* [27]. For their ground-state calculations, they used the accurate potential by Umrigar and Gonze [21] and for the xc-kernel they used the ALDA. The calculations were

TABLE IV: The  $\mu_i$  from different ground-state potentials for He, Be, and Ne. The ionization energies are in [a.u.] and are not included in the maximum error.

		$s$			$p$		
		OEP	LB94	exact	OEP	LB94	exact
He	$I$	0.9182	0.8513	0.9037			
	$\mu_0$	0.2170	-0.3607	0.2139	0.0238	-0.6015	0.0164
	$\mu_1$	-0.0401	-2.7408	-0.0370	0.0319	-2.2013	0.0289
	$\mu_2$		-3.1852			-1.5723	
	Max. AE	0.0000	0.003	0.0006	0.0000	0.002	0.0009
Be	$I$	0.3093	0.3205	0.3426			
	$\mu_0$	0.6623	0.3497	0.7164	0.2786	0.0115	0.3287
	$\mu_1$	-0.1557	-0.7203	-0.2185	-0.1070	0.4836	-0.3377
	$\mu_2$		31.5313		0.8453	66.0517	0.6112
	$\mu_3$		73.1572			268.6094	
	Max. AE	0.0002	0.001	0.0002	0.0002	0.002	0.0003
Ne	$I$	0.8508	0.7821	0.7945			
	$\mu_0$	1.3433	0.8174	1.3125	0.8631	0.3196	0.8340
	$\mu_1$	-0.2285	-3.2880	-0.1807	-0.3972	-2.8338	-0.3500
	$\mu_2$		-11.0968			-1.3271	
	$\mu_3$		-39.2359				
	Max. AE	0.0004	0.004	0.0007	0.0008	0.003	0.001

TABLE V: Transition energies for the beryllium atom.

Transition	Expt. <sup>a</sup>	KS <sup>b</sup>	ALDA <sup>c</sup>	Truncated-ALDA <sup>d</sup>	Truncated-Hybrid <sup>e</sup>	WY <sup>f</sup>	AC-LDA <sup>g</sup>
$2s \rightarrow 3s$	0.24913	0.24437	0.2495	0.2515	0.2510	0.2512	0.2239
$2s \rightarrow 4s$	0.29728	0.29586	0.2977	0.2984	0.2985	0.3033	0.2680
$2s \rightarrow 5s$	0.31586	0.31526	0.3160	0.3164	0.3165		
$2s \rightarrow 6s$	0.32496	0.32466		0.3252	0.3254		
$2s \rightarrow 2p$	0.19394	0.13273	0.1868	0.1889	0.1427	0.1861	0.1781
$2s \rightarrow 3p$	0.27423	0.26937	0.2710	0.2714	0.2736	0.2749	0.2457
$2s \rightarrow 4p$	0.30543	0.30461	0.3048	0.3049	0.3059	0.3107	0.2754
$2s \rightarrow 5p$	0.31949	0.31931		0.3194	0.3199		
$2s \rightarrow 6p$	0.32690	0.32686		0.3269	0.3272		
$s$ MAE [mH]			0.312	1.069	0.943	4.046	27.25
$p$ MAE [mH]			3.669	1.700	10.61	4.592	24.81
Total MAE [mH]			1.991	1.420	6.313	4.374	25.79

<sup>a</sup>Experimental values from NIST [26]

<sup>b</sup>The differences between the KS eigenvalues obtained with the exact potential from Ref. [21]

<sup>c</sup>ALDA calculation including all bound and unbound states from Ref. [27]

<sup>d</sup>ALDA calculation including 34 unbound states from Ref. [28]

<sup>e</sup>Hybrid calculation including 34 unbound states for He and 38 unbound states for Be from Ref. [29]

<sup>f</sup>ALDA calculation with WY ground-state potential from Ref. [30]

<sup>g</sup>Asymptotically corrected ALDA results from Ref. [30]

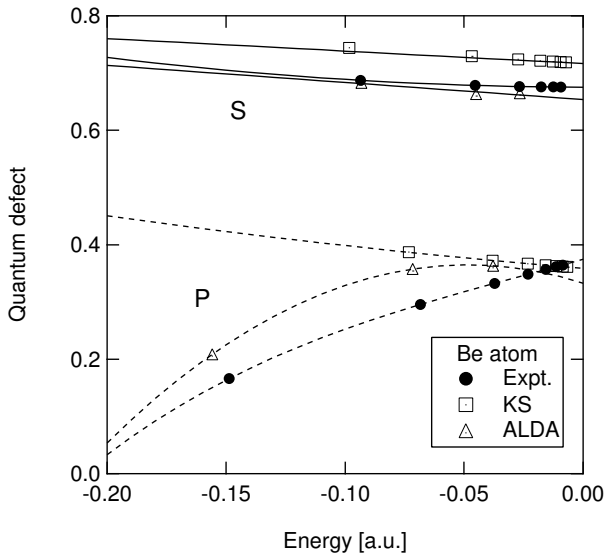
done close to the basis set limit and with high numerical integration accuracy. As can be seen from the table the excitation energies for the  $s \rightarrow s$  transitions are very close to the experimental values with a mean average error (MAE) of only 0.3 mH. The  $s \rightarrow p$  excitation energies are a bit less accurate with an MAE of 3.7 mH, but this is still an accurate result. The fit coefficients for the quantum defects of these calculations are reported in

Table VI. For the fit of the TDDFT results we took a less strict constraint to determine when to stop adding more coefficients. We took 0.01 instead of 0.001, reflecting the greater error in this data.

In Fig. 6 we show the  $s$  and  $p$  quantum defects corresponding to these values and we compare them with the bare KS and experimental results. For the  $s$  quantum defect, the experimental curve is essentially a straight

TABLE VI: The  $\mu_i$  from different singlet TDDFT values for Be.

	Ref. <sup>a</sup>	KS <sup>b</sup>	ALDA <sup>c</sup>	Truncated-ALDA <sup>d</sup>	Truncated-Hybrid <sup>e</sup>	WY/ALDA <sup>f</sup>	AC-LDA <sup>g</sup>
<i>s</i>							
$I$	0.3426	0.3426	0.3426	0.3426	0.3426	0.3493	0.3111
$\mu_0$	0.6752	0.7164	0.6536	0.6182	0.6010	0.6684	0.5997
$\mu_1$	-0.0133	-0.2185	-0.2986	-0.4294	-0.6947	-0.7540	
$\mu_2$	1.2345						
Max. AE	0.0003	0.0002	0.004	0.002	0.004	0.0000	0.006
<i>p</i>							
$\mu_0$	0.3745	0.3287	0.3327	0.3427	0.3087	0.3484	0.2413
$\mu_1$	1.1612	-0.3377	-1.3172	-0.9634	0.2505	-1.9702	-1.1215
$\mu_2$	1.5678	0.6112	-13.5673	-12.4534	3.9961	-15.7792	-18.6196
$\mu_3$	21.4587						
Max. AE	0.0002	0.0003	0.0000	0.003	0.004	0.0000	0.0000

<sup>a</sup>Experimental values from NIST [26]<sup>b</sup>The differences between the KS eigenvalues obtained with the exact potential from Ref. [21]<sup>c</sup>ALDA calculation including all bound and unbound states from Ref. [27]<sup>d</sup>ALDA calculation including 34 unbound states from Ref. [28]<sup>e</sup>Hybrid calculation including 38 unbound states from Ref. [29]<sup>f</sup>ALDA calculation with WY ground-state potential from Ref. [30]<sup>g</sup>Asymptotically corrected ALDA results from Ref. [30]FIG. 6: The  $s$  and  $p$  experimental, KS, and ALDA singlet quantum defects for Be. The continuous lines are the  $\mu^{(p)}(E)$  fits.

line, with a small negative slope. The  $p$  quantum defect, on the other hand, is much more curved, with a large positive slope, due to the much lower  $2s \rightarrow 2p$  transition. The exact KS potential has been touted as a good approximation to the experimental results [31]. This is clearly true for the  $s$  curves but not so for the  $p$  quantum defect. In that case the KS quantum defect, while being very close to the experimental value as  $n \rightarrow \infty$  has the wrong behavior as a function of  $E$ .

In both the  $s$  and  $p$  case it is clear that doing a full

TDDFT calculation considerably improves upon the bare KS results. The ALDA does slightly overcorrect the  $s$  quantum defect, underestimating the value at  $E = 0$ . In case of the  $p$  quantum defect the ALDA tends to correct for the opposite slope of the KS values compared to the experimental values, but the correction is not complete, leading to a curved line. We also see that the  $s$  quantum defects as obtained with the ALDA are much better than the  $p$  quantum defects, even though the MAE is only a few mH in the last case.

## B. Truncating Casida's equation

Another set of ALDA calculations were performed by Petersilka, Gross, and Burke [28]. The difference between their calculation and that of Van Gisbergen is that they truncate the summation over states in the response function, including only poles of bound states and neglecting continuum contributions. They included the lowest 34 bound states of  $s$  and  $p$  symmetry in their calculations. Just like in case of the full ALDA calculations the ground-state was determined with the potential of Umrigar and Gonze [21]. We show these results in column four of Table V. Again the results are close to the experimental values with an MAE of 1.1 mH for the  $s \rightarrow s$  transitions and an MAE of 1.7 mH for the  $s \rightarrow p$  transitions. In Fig. 7 we show the  $s$  and  $p$  quantum defects corresponding to these values and we compare them with the full ALDA results. For the  $s$  quantum defect we see that the quantum defect is slightly below the ALDA values, and the slope is too large, leading to a smaller asymptotic quantum defect. For the  $p$  quantum defect we see that there is not much difference between the truncated and the full

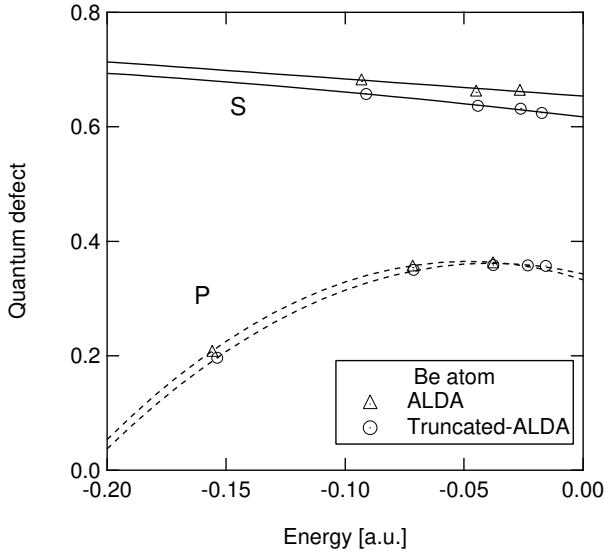


FIG. 7: The  $s$  and  $p$  ALDA and truncated-ALDA singlet quantum defects for Be. The continuous lines are the  $\mu^{(p)}(E)$  fits.

results. So the effect of the truncation in case of Be is not so great. For He the difference is relatively larger, because the TDDFT corrections are so small. This can be seen from the values in Tables VI and VII, which we will discuss in section IV F.

### C. Quality of the ground-state potential

For all TDDFT methods we have described so far, the ground-state was calculated with the exact potential of Umrigar and Gonze [21]. This eliminates errors in the ground-state so one can compare the effects of using a different xc-kernel. But for practical calculations such an accurate potential is not available. This motivates the development of other accurate ground-state potentials to calculate the Rydberg series.

Wu and Yang [12] obtained an accurate potential by a direct optimization method that allows them to calculate the potential from a given electronic density. This density is obtained from a coupled-cluster singles and doubles (CCSD) calculation. In Table V we show the excitation energies corresponding to the WY potentials and the error is just a few mH. In Fig. 8 we show the quantum defects obtained with this potentials and compare them with the ALDA and experimental values. Only the asymptotic value of the quantum defect is accurate. Errors due to (very small) errors in the ground-state density are visible for all other energies, and can be comparable to the xc-kernel itself. The WY method is therefore still very promising, but clearly requires a very accurate input density. Quantum defect analysis should prove very useful for testing WY-type calculations, for example, for comparing basis set errors with errors due to the level of

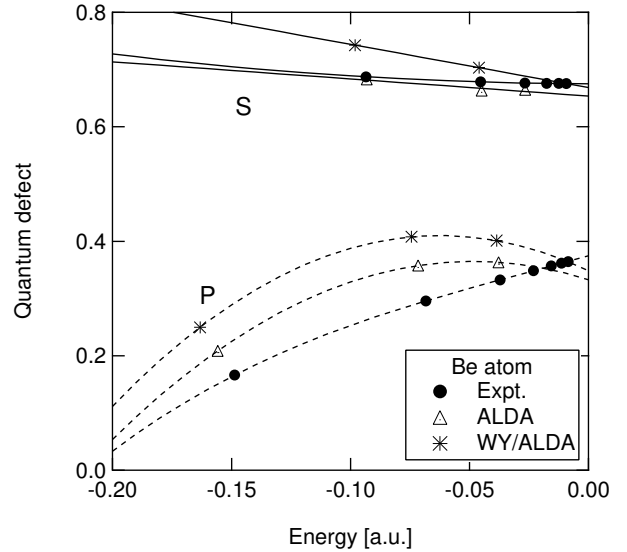


FIG. 8: The  $s$  and  $p$  experimental, ALDA, and WY quantum defects for Be. The continuous lines are the  $\mu^{(p)}(E)$  fits.

calculation used for obtaining the input density.

### D. Testing approximate kernels

In an attempt to improve the xc-kernel, Burke, Peterilka, and Gross [29] suggested the following form,

$$f_{xc}^{\uparrow\uparrow} = f_x^{\uparrow\uparrow}, \quad f_{xc}^{\uparrow\downarrow} = f_{xc}^{\uparrow\downarrow\text{ALDA}}. \quad (3)$$

This form is based on the fact that the parallel-spin contribution is well described in the exact exchange case, because of a cancellation of exchange contributions. But an exact exchange treatment misses the significant anti-parallel correlation contribution, leading to too large singlet/triplet splittings. Therefore it is recommended that for the anti-parallel kernel one uses the ALDA. We show the excitation energies obtained with this kernel in Table V. It should be noted that just as in case of the truncated-ALDA calculations, the number of states included in the hybrid calculation is also limited. Namely, 34 states in case of He and 38 states in case of Be. Therefore we shall denote the method by truncated-hybrid. The ground-state of these calculations was again calculated with the exact potential of Umrigar and Gonze [21]. Apart from the  $2s \rightarrow 2p$  transition the truncated-hybrid results are very similar to the truncated-ALDA results. It is the large error in the  $2s \rightarrow 2p$  transition that leads to the large MAE.

In Fig. 9 we show the  $s$  and  $p$  quantum defects corresponding to the truncated-hybrid results and we compare them with the truncated-ALDA and experimental results. From the  $s$  quantum defect plot it can again be seen that the truncated-hybrid results are close to the truncated-ALDA values, so the kernel does not improve

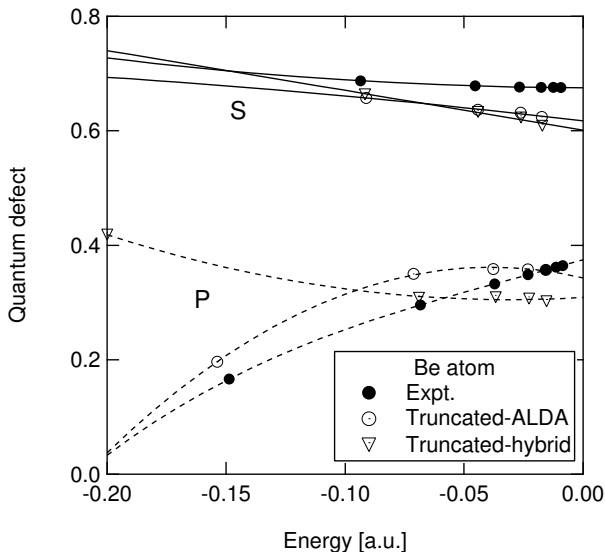


FIG. 9: The  $s$  and  $p$  experimental, truncated-ALDA, and truncated-hybrid singlet quantum defects for Be. The continuous lines are the  $\mu^{(p)}(E)$  fits.

the results in this case. For the  $p$  quantum defect, the results actually get worse with the truncated-hybrid giving a slope opposite the the experimental curve, so it shifts the KS values in the right direction but does not correct for the wrong slope. The hybrid kernel does not improve much upon the truncated-ALDA for Be as was also found in Ref. [29]. It is only good for two-electron systems, for which it was derived.

### E. Asymptotically corrected ground-state potentials

Wu, Ayers, and Yang [25] obtained an asymptotically corrected LDA (AC-LDA) potential by a variational method that forces the potential to have the correct asymptotic behavior. This is a pure DFT treatment that can be applied to larger molecules. We see from Table V that the AC-LDA gives a large MAE.

In Fig. 10 we show the quantum defects obtained with the AC-LDA potential and compare them with the KS and experimental values. In both cases the AC-LDA values are much lower than the ALDA, which was evaluated on the exact ground-state KS potential. The AC-LDA strongly underestimates the experimental  $s$  and  $p$  quantum defects. The shape of the  $p$  curve is similar to the ALDA curve. From this figure, it is clear that there are significant errors in the underlying KS potential.

### F. Coefficients for He

In this section we give the values of the best fit for He as defined in Eq. 2 and as described thereafter. The

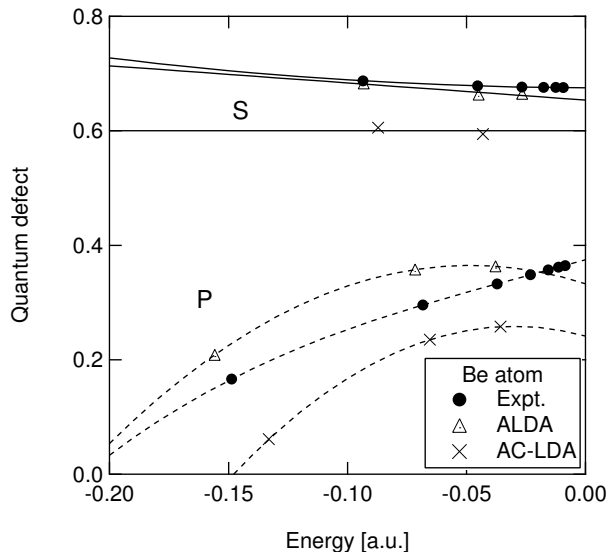


FIG. 10: The  $s$  and  $p$  experimental, ALDA, and AC-LDA quantum defects for Be. The continuous lines are the  $\mu^{(p)}(E)$  fits.

original excitation energies from which the quantum defects and corresponding coefficients are calculated are obtained from the same sources as the Be data described above. In Table VII, we give results for He. The sizes of the quantum defects are much smaller than in Be, and the fractional change between KS and experiment is concomitantly larger. In the case of the  $p$  quantum defects, they can have large opposite signs. Application of ALDA to the exact ground-state KS potential again works well.

In the case of He, the truncated-hybrid result improves upon the truncated-ALDA. As we mentioned before this is because the hybrid was developed for 2-electron systems. AC-LDA and WY coefficients of He really stand out as behaving much differently from the other cases and giving large errors that cannot be removed by adding more coefficients. The AC-LDA and WY coefficients of Be did not have this problem.

### G. Triplets

In practice, spin decomposed TDDFT is commonly used, and allows prediction of singlet $\rightarrow$ triplet transitions. In this section we discuss the coefficients of the quantum defect expansion obtained from triplet excitation energies. In Table VIII we show the fit coefficients for He and Be. For the WY and AC-LDA methods there is no triplet data available. For the triplet case, the  $\mu_0$ 's are very well reproduced in all cases, also the other coefficients are often close. Overall the data can in most cases be reproduced by only two or three coefficients.



TABLE VII: The  $\mu_i$  from different singlet TDDFT values for He.

	Ref. <sup>a</sup>	KS <sup>b</sup>	ALDA <sup>c</sup>	Truncated-ALDA <sup>d</sup>	Truncated-Hybrid <sup>e</sup>	WY/ALDA <sup>f</sup>	AC-LDA <sup>g</sup>
<i>s</i>							
<i>I</i>	0.9037	0.9037	0.9037	0.9037	0.9037	0.9026	0.7817
$\mu_0$	0.1395	0.2139	0.1099	0.0223	0.0599	0.0226	-0.1027
$\mu_1$	-0.0655	-0.0370	-0.1388	-0.4537	-0.5390	-2.4879	-4.3920
$\mu_2$					-12.6664	-25.7710	
Max. AE	0.0002	0.0006	0.001	0.006	0.007	0.03	0.06
<i>p</i>							
$\mu_0$	-0.0122	0.0164	-0.0002	-0.0168	-0.0355	-0.1039	-0.1579
$\mu_1$	-0.0227	0.0289	-0.2077	-0.2721	-0.2201	-6.1973	-2.0656
$\mu_2$					-107.6068	-13.2488	
$\mu_3$					-521.8636		
Max. AE	0.0001	0.0009	0.005	0.002	0.008	0.007	0.02

<sup>a</sup>Non-relativistic calculations from Ref. [16]<sup>b</sup>The differences between the KS eigenvalues obtained with the exact potential of Ref. [17].<sup>c</sup>ALDA calculation including all bound and unbound states from Ref. [27]<sup>d</sup>ALDA calculation including 34 unbound states from Ref. [28]<sup>e</sup>Hybrid calculation including 34 unbound states from Ref. [29]<sup>f</sup>ALDA calculation with WY ground-state potential from Ref. [30]<sup>g</sup>Asymptotically corrected ALDA results from Ref. [30]TABLE VIII: The  $\mu_i$  from different triplet TDDFT values for He and Be.

	Ref. <sup>a</sup>	ALDA <sup>b</sup>	Truncated-ALDA <sup>c</sup>	Truncated-Hybrid <sup>d</sup>
<i>s</i>				
He $\mu_0$	0.2965	0.2719	0.2570	0.3171
$\mu_1$	-0.0811	-0.0892	-0.1281	
Max. AE	0.0001	0.004	0.003	0.007
Be $\mu_0$	0.7742	0.7706	0.7641	0.7683
$\mu_1$	0.8870	-0.3912	-0.4015	-0.2607
Max. AE	0.001	0.0003	0.002	0.002
<i>p</i>				
He $\mu_0$	0.0684	0.0734	0.0657	0.05332
$\mu_1$	0.0457			0.1103
Max. AE	0.0002	0.003	0.005	0.002
Be $\mu_0$	0.3620	0.4152	0.4101	0.37852
$\mu_1$	-0.4492	0.3553	-0.7166	-0.6404
$\mu_2$	1.5829			1.5225
Max. AE	0.0003	0.004	0.006	0.007

<sup>a</sup>He non-relativistic calculations from Ref. [16] and Be and Ne experimental values from NIST [26]<sup>b</sup>ALDA calculation including all bound and unbound states from Ref. [27]<sup>c</sup>ALDA calculation including 34 unbound states from Ref. [28]<sup>d</sup>Hybrid calculation including 34 unbound states for He and 38 unbound states for Be from Ref. [29]

## V. CONCLUSIONS

In the first part of this paper we have shown that the quantum defect is a valuable quantity when reporting Rydberg states. A plot of the quantum defect can be more insightful than a list of excitation energies. The quantum defect can also be fitted to an expansion around  $E = 0$  and a finite number of expansion coefficients can fully

describe the Rydberg series. We calculated the quantum defects for He, Be, and Ne with accurate xc-potentials and showed that the KS quantum defect lies between the interacting singlet and triplet values.

We also studied approximate ground-state KS potentials, namely, the LB94 and OEP potentials. We saw that the OEP results are very close to the exact KS values. The LB94 underestimates the quantum defect in all cases. Again the data can be fully described by a few coefficients.

In the final part of the paper we calculated the quantum defects from available TDDFT excitation energies from the literature. We see that the quantum defect really amplifies the error in these cases. The TDDFT data can be described by only a few coefficients.

Overall we see that while having an asymptotically correct potential guarantees the existence of a Rydberg series, it is not necessarily a good one. This is especially the case for AC-LDA TDDFT and LB94 ground state values, and to lesser extent even for the WY TDDFT values.

## Acknowledgments

We thank Qin Wu for providing the ionization energies corresponding to their AC-LDA and WY calculations. We also thank Robert van Leeuwen for useful discussions. This work was supported by NSF Grant No. CHE-0355405.

- 
- [1] E. Runge and E. K. Gross, *Density-Functional Theory for Time-Dependent Systems*, Phys. Rev. Lett. **52**, 997 (1984).
- [2] F. Furche and D. Rappoport, in *Computational Photochemistry*, edited by M. Olivucci (to be published, Elsevier, Amsterdam, 2005).
- [3] K. Burke, J. Werschnik, and E. K. U. Gross, *Time-dependent density functional theory: Past, present, and future*, J. Chem. Phys. **123**, 062206 (2005).
- [4] M. van Faassen and P. L. de Boeij, *Excitation energies for a benchmark set of molecules obtained within time-dependent current-density functional theory using the Vignale-Kohn functional*, J. Chem. Phys. **120**, 8353 (2004).
- [5] M. Petersilka, U. J. Gossmann, and E. K. U. Gross, *Excitation Energies from Time-Dependent Density-Functional Theory*, Phys. Rev. Lett. **76**, 1212 (1996).
- [6] M. Levy, J. P. Perdew, and V. Sahni, *Exact Differential Equation for the Density and Ionization Energy of a Many-Particle System*, Phys. Rev. A **30**, 2745 (1984).
- [7] C. O. Almbladh and A. C. Pedroza, *Density-functional exchange-correlation potentials and orbital eigenvalues for light atoms*, Phys. Rev. A **29**, 2322 (1984).
- [8] A. Mattsson, *In pursuit of the "Devine" functional*, Science **298**, 5594 (2002).
- [9] R. van Leeuwen and E. J. Baerends, Phys. Rev. A **49**, 2421 (1994).
- [10] D. J. Tozer and H. N. C., *Improving virtual Kohn-Sham orbitals and eigenvalues: Application to excitation energies and static polarizabilities*, J. Chem. Phys. **109**, 10180 (1998).
- [11] M. E. Casida and D. R. Salahub, *Asymptotic correction approach to improving approximate exchange-correlation potentials: Time-dependent density-functional theory calculations of molecular excitation spectra*, J. Chem. Phys. **113**, 8918 (2000).
- [12] Q. Wu and W. Yang, *A direct optimization method for calculating density functionals and exchange-correlation potentials from electron densities*, J. Chem. Phys. **118**, 2498 (2003).
- [13] H. Friedrich, *Theoretical Atomic Physics* (Springer-Verlag, 1998), 2nd ed.
- [14] A. I. Al-Sharif, R. Resta, and C. J. Umrigar, *Evidence of physical reality in the Kohn-Sham potential: The case of atomic Ne*, Phys. Rev. A **57**, 2466 (1998).
- [15] M. J. Seaton, *The Quantum Defect Method*, Mon. Not. R. Astron. Soc. **188**, 504 (1955).
- [16] G. W. F. Drake, in *Atomic, Molecular, and Optical Physics Handbook*, edited by G. W. F. Drake (AIP Press, Woodbury, NY, 1996), p. 154.
- [17] C. J. Umrigar and X. Gonze, *Accurate exchange-correlation potentials and total-energy components for the helium isoelectronic series*, Phys. Rev. A **50**, 3827 (1994).
- [18] prof. dr. E. Engel: engel@th.physik.uni-frankfurt.de.
- [19] E. Engel and R. M. Dreizler, *From explicit to implicit density functionals*, J. Comput. Chem. **20**, 31 (1999).
- [20] J. D. Talman and W. G. Shadwick, Phys. Rev. A **14**, 36 (1976).
- [21] C. J. Umrigar and X. Gonze, in *High Performance Computing and its Application to the Physical Sciences*, edited by D. A. Browne *et al.* (World Scientific, Singapore, 1993), vol. 94.
- [22] A. Görling, *A new KS method for molecules based on an exchange charge density generating the exact local KS exchange potential*, Phys. Rev. Lett. **83**, 5459 (1999).
- [23] S. Ivanov, S. Hirata, and J. Bartlett, *Exact exchange treatment for molecules in finite-basis-set Kohn-Sham theory*, Phys. Rev. Lett. **83**, 5455 (1999).
- [24] M. Grüning, O. V. Gritsenko, S. J. A. van Gisbergen, and E. J. Baerends, J. Chem. Phys. **112**, 652 (2001).
- [25] Q. Wu, P. W. Ayers, and W. Yang, *Density functional theory calculations with correct long-range potentials*, J. Chem. Phys. **119**, 2978 (2003).
- [26] NIST Atomic Spectra Database, URL <http://physics.nist.gov/PhysRefData/ASD/index.html>.
- [27] S. J. A. van Gisbergen, F. Kootstra, P. R. T. Schipper, O. V. Gritsenko, J. G. Snijders, and E. J. Baerends, *Density-functional-theory response-property calculations with accurate exchange-correlation potentials*, Phys. Rev. A **57**, 2666 (1998).
- [28] M. Petersilka, E. K. U. Gross, and K. Burke, *Excitation Energies from Time-Dependent Density Functional Theory Using Exact and Approximate Potentials*, Int. J. Quant. Chem. **80**, 534 (2000).
- [29] K. Burke, M. Petersilka, and E. K. U. Gross, in *Recent Advances in Density Functional Methods*, edited by V. Barone, P. Fantucci, and A. Bencini (World Scientific, 2000), vol. 3, pp. 67–79.
- [30] Q. Wu, A. J. Cohen, and W. Yang, *Excitation energies from time-dependent density functional theory with accurate exchange-correlation potentials*, Mol. Phys. **103**, 711 (2005).
- [31] A. Savin, C. J. Umrigar, and X. Gonze, *Relationship of Kohn-Sham eigenvalues to excitation energies*, Chem. Phys. Lett. **288**, 391 (1998).